Diffusion Monte Carlo study of circular quantum dots

Francesco Pederiva
Dipartimento di Fisica and INFM, Università di Trento, I-38050 Povo, Trento, Italy

C. J. Umrigar
Cornell Theory Center, Cornell University, Ithaca, New York 14853

E. Lipparini
Dipartimento di Fisica and INFM, Università di Trento, I-38050 Povo, Trento, Italy
(Received 14 March 2000)

We present ground- and excited-state energies obtained from diffusion Monte Carlo (DMC) calculations, using accurate multiconfiguration wave functions, for N electrons ($N \leqslant 13$) confined to a circular quantum dot. We compare the density and correlation energies to the predictions of local spin density approximation (LSDA) theory and Hartree-Fock (HF) theory, and analyze the electron-electron pair-correlation functions. The DMC estimated change in electrochemical potential as a function of the number of electrons in the dot is compared to that from LSDA and HF calculations. Hund's first rule is found to be satisfied for all dots except $N=4$ for which there is a near degeneracy.

I. INTRODUCTION

Modern microfabrication technology is capable of making quantum dots[1,2] that are sufficiently small that they contain only a small number of mobile electrons. There has been much interest in studying the atomiclike properties of these dots with tunnel conductance[3] and capacitance[4] experiments. The ground states of clean circular dots exhibit shell structure and are believed to obey Hund's first rule.[5,6] The shell structure is particularly evident in measurements of the change in electrochemical potential due to the addition of one extra electron, $\Delta_N = \mu(N+1) - \mu(N)$, where N is the number of electrons in the dot, and $\mu(N) = E(N) - E(N-1)$ is the electrochemical potential of the system. Theoretical predictions of Δ_N and the excitation energy spectrum require accurate calculations ground-state and excited-state energies. Exact diagonalization studies[7,8] are accurate for a very small number of electrons, but the number of basis functions needed to obtain a given accuracy and the computational cost grow very rapidly with electron number. In practice they have been used for up to eight electrons,[7,8] but the accuracy is very limited for all except $N \leqslant 3$. Hartree,[9] restricted Hartree-Fock (HF), spin and/or space unrestricted Hartree-Fock[10–12] (UHF), and local spin-density approximation (LSDA) and current density functional methods[13–15] give results that are satisfactory for a qualitative understanding of some systematic properties. However, comparisons with exact results show discrepancies in the energies that are substantial on the scale of energy differences. An advantage of the approximate approaches is that no serious size and geometry constraints are imposed.

In this paper we employ the quantum Monte Carlo (QMC) method [both variational Monte Carlo (VMC) and diffusion Monte Carlo (DMC) methods] because they yield very accurate energies at a computational cost that grows relatively modestly with the number of electrons. The statistical error of these calculations can be made small, even for dots with several tens of electrons, within a reasonable amount of computer time on a modern workstation. In addition to the statistical error there is a systematic error due to using the fixed-node approximation. This error can be reduced by optimizing the trial wave functions. For the trial wave functions used in the present work, the fixed-node errors are small compared to the errors of other approximate methods. This is demonstrated by performing internal checks within the method and by comparing to the few energies, available from exact diagonalization studies[7,8] for small dots, that are accurate enough to make a meaningful comparison. Hence our results can be regarded as a benchmark to assess the accuracy of other approximate methods. In particular we find that, in contrast to the situation with atoms, the energies obtained from the LSDA method are considerably more accurate than those from the HF method. The same is true for the spin densities in those cases where the LSDA wave functions are eigenstates of the total spin operator $\hat{S}^2$.

Earlier QMC calculations on quantum dots include VMC calculations for circular dots[17] and DMC calculations for three-dimensional dots.[18] The fixed-phase DMC method has been applied to dots[19] with $N \leqslant 4$. Path integral Monte Carlo calculations have been performed[20] for dots with $N \leqslant 8$ but the results of these calculations bear no resemblance to either our results or those from exact diagonalization.[7,8]

II. COMPUTATIONAL METHOD

A. Hamiltonian

The usual model[2] for a disk-shaped vertical quantum dot is a two-dimensional system of N electrons moving in the $z=0$ plane, confined by a parabolic lateral confining potential $V_{\rm con}(\mathbf{r})$. The Hamiltonian is

$$H = \sum_{i=1}^{N} \left(-\frac{\hbar^2}{2m^*}\nabla_i^2 + V_{\rm con}(\mathbf{r}_i) \right) + \frac{e^2}{\epsilon} \sum_{i<j}^{N} \frac{1}{|\mathbf{r}_i - \mathbf{r}_j|}. \quad (1)$$

In Eq. (1), m^* is the electron effective mass, and ϵ is the dielectric constant of the semiconductor. In the following (if not explicitly specified otherwise) we will use effective atomic units, defined by $\hbar = e^2/\epsilon = m^* = 1$. In this system of units, the length unit is the Bohr radius a_0 times $\epsilon m_e/m^*$, and the energy unit is the Hartree times $m^*/(m_e\epsilon^2)$. For the GaAs dots we consider here, $\epsilon = 12.4$ and $m^* = 0.067 m_e$, and the effective Bohr radius a_0^* and effective Hartree H* are $\simeq 97.93$ Å and $\simeq 11.86$ meV, respectively. In this first application of the method, we will consider circular dots with $N \leqslant 13$ and a parabolic potential $V_{\rm con}(\mathbf{r}) = m^*\omega^2 r^2/2$ ($\hbar\omega = 0.28$ H* $= 3.32$ meV), which should approximate the experimental situation in Ref. 5. Extensions of the calculation to $N > 13$, magnetic field $B \neq 0$, and a nonparabolic confining potential are in progress.

Comparison of energies and other quantities with those in the literature are complicated by the fact that various authors use different values for the parameters, m^*, ϵ, ω in the Hamiltonian. Note, however, that two Hamiltonians H_1 and H_2, characterized by m_1^*, ω_1, and ϵ_1 and m_2^*, ω_2, and ϵ_2, respectively, must have the same energy spectrum aside from a multiplicative scale factor, i.e., $E_{1i}/E_{2i} = m_2^*/m_1^* = \omega_1/\omega_2 = \epsilon_2/\epsilon_1$, where i labels the energy states of a given Hamiltonian. An interesting aspect of quantum dots is that it is possible to tune λ, the dimensionless ratio of the Coulomb interaction strength to the confining potential $\lambda = [e^2/(\epsilon l_0)]/\hbar\omega$, where $l_0 = \sqrt{\hbar/(m^*\omega)}$, thereby allowing one to study both weakly interacting and strongly interacting cases. Our present calculations are for $\lambda = 1.89$.

B. Quantum Monte Carlo methods

One advantage of the QMC methods is that no restriction is placed on the form of the trial wave function. In the VMC method, Monte Carlo integration is used to calculate the many-dimensional integrals, and the parameters in the trial wave function can be varied to minimize the energy or the fluctuations of the local energy. More accurate results can be obtained from the fixed-node diffusion Monte Carlo method which projects, from an antisymmetric trial wave function, the lowest-energy state, consistent with the boundary condition of preserving the same nodal surface. In the limit that the trial wave function has the correct nodes, the fixed-node DMC method yields the exact energy with only a statistical error that can be made arbitrarily small by increasing the number of Monte Carlo steps. A detailed description of our implementation can be found in Ref. 21. The fixed-node error is usually small compared to errors from other methods but it is unknown except in those cases where exact results are available.

C. Trial wave functions

The errors of VMC and fixed-node DMC calculations depend on the quality of the trial wave functions. The trial wave functions we use have the form

$$\Psi(\mathbf{R})_{L,S} = \exp[\phi(\mathbf{R})] \sum_{i=1}^{N_{\rm conf}} \alpha_i \Xi_i^{L,S}(\mathbf{R}), \tag{2}$$

where $\mathbf{R} = \{\mathbf{r}_1 \cdots \mathbf{r}_N\}$ are the coordinates of the N electrons in the dot, and the α_i are variational parameters. The configuration-state functions $\Xi^{L,S}$ are eigenstates of the total angular momentum $\hat{L} \equiv \hat{L}_z$ with eigenvalue L and of the total spin $\hat{S}^2$ with eigenvalue $S(S+1)$, and have the following form:

$$\Xi_i^{L,S} = \sum_{j=1}^{m_i} \beta_j D_j^{\uparrow} D_j^{\downarrow}, \tag{3}$$

where the D_j^{χ} are Slater determinants of spin-up and spin-down electrons, using orbitals from a local density approximation (LDA) calculation with the same confining potential and the same number of electrons. The m_i are the number of determinants in the ith configuration. In general the $D_j^{\uparrow} D_j^{\downarrow}$ are not eigenstates of $\hat{S}^2$. The coefficients β in the linear combination of Eq. (3) are fixed by diagonalizing $\hat{S}^2$ in that determinantal basis. For $N \leqslant 13$, the number of configurations, $N_{\rm conf}$, and Slater determinants $N_{\rm det} = \sum_{i=1}^{N_{\rm conf}} m_i$, appearing in Eqs. (2) and (3), are shown in Table I and were determined by limiting the basis space to spin-up and spin-down orbitals with $|n,l\rangle = |0,0\rangle$ for $N \leqslant 2$ dots, $|n,l\rangle = |0,0\rangle$ and $|0,\pm 1\rangle$ for $3 \leqslant N \leqslant 6$ dots, $|n,l\rangle = |0,0\rangle$, $|0,\pm 1\rangle$, $|0,\pm 2\rangle$, and $|1,0\rangle$ for $7 \leqslant N \leqslant 12$ dots, and $|n,l\rangle = |0,0\rangle$, $|0,\pm 1\rangle$, $|0,\pm 2\rangle$, $|1,0\rangle$, $|0,\pm 3\rangle$, and $|1,\pm 1\rangle$ for the $N = 13$ dot. The noninteracting single-particle energy levels are $\epsilon_{n,l} = (2n + |l| + 1)\omega$.[22] Basis states are then built by considering all possible occupations of open-shell levels. For example, in the case of the $N = 9$ dot, the first six electrons fill the $|0,0\rangle$ and $|0,\pm 1\rangle$ orbitals and are considered to be core electrons in a closed shell. Then, the wave function for the state $|L = 0, S = 1/2\rangle$ of the $N = 9$ dot has three open-shell electrons, and includes two ($N_{\rm conf} = 2$) configuration-state functions which are linear combinations of $m_1 = 2$ and $m_2 = 3$ Slater determinants, respectively.

The function $\exp[\phi]$ in Eq. (2) is a generalized Jastrow factor of the form used in Ref. 23,

$$\phi(R) = \sum_{i=1}^{N} \left[\sum_{k=1}^{6} \gamma_k J_0\left(\frac{k\pi r_i}{R_c}\right) \right] + \sum_{i<j}^{N} \frac{1}{2}\left(\frac{a_{ij} r_{ij}}{1 + b(r_i) r_{ij}} + \frac{a_{ij} r_{ij}}{1 + b(r_j) r_{ij}} \right), \tag{4}$$

where

$$b(r) = b_0^{ij} + b_1^{ij} \tan^{-1}[(r - R_c)^2/2R_c\Delta]. \tag{5}$$

It explicitly includes one- and two-body correlations and effective multibody correlations through the spatial dependence of $b(r)$. The quantity R_c represents an ''effective'' radius of the dot, and has been assumed to be equal to $1.93\sqrt{N}$. The b_0 and b_1 parameters depend only on the *relative* spin configuration of the pair ij. The parameters a_{ij} are fixed in order to satisfy the cusp conditions, that is, the condition of finiteness of the local energy $\hat{H}\Psi/\Psi$ for $r_{ij} \to 0$. For a two-dimensional system, $a_{ij} = 1$ if the electron pair ij has antiparallel spin, and $a_{ij} = 1/3$ otherwise. The dependence of a_{ij} on the relative spin orientation of the electron pair introduces spin contamination into the wave func-

TABLE I. Ground-state energies (in H*) and low-lying excitation energies (in mH*) for $N \leq 13$ dots. Also shown are the quantum numbers of the states and the number of configuration state functions, $N_{\rm conf}$, and the number of determinants, $N_{\rm det}$, used in constructing them. The numbers in parentheses are the statistical uncertainties in the last digit.

N	L	S	$N_{\rm conf}$	$N_{\rm det}$	E(H*), ΔE(mH*)
2	0	0	1	1	1.02162(7)
3	1	1/2	1	1	2.2339(3)
4	0	0	1	2	3.7135(4)
	0	1	1	1	2.2(6)
	2	0	1	1	41(1)
5	1	1/2	1	1	5.5336(3)
6	0	0	1	1	7.5996(8)
7	2	1/2	1	1	10.0361(8)
	0	1/2	1	1	24(1)
8	0	1	1	1	12.6903(7)
	2	1	1	2	22(1)
	2	0	1	2	24(1)
	4	0	1	1	32(1)
	0	0	2	3	54(1)
9	0	3/2	1	1	15.5784(7)
	0	1/2	2	5	43(1)
	2	1/2	2	2	52(1)
	4	1/2	1	1	67(1)
10	2	1	1	2	18.7244(5)
	2	0	1	2	2(1)
	0	1	1	1	22(1)
	0	0	2	3	26(1)
	4	0	1	1	45(1)
11	0	1/2	1	1	22.0750(4)
	2	1/2	1	1	14(1)
12	0	0	1	1	25.6548(7)
13	3	1/2	1	1	29.4942(7)
	1	1/2	1	1	40(1)

tion. However, the magnitude of the spin contamination and its effect on the energy has been shown to be totally negligible in the case of well-optimized atomic wave functions[24] and we expect that to be true here as well.

The coefficients γ_k in the one-body term, the coefficients Δ, b_0, and b_1 in the two-body term, and the coefficients α_i multiplying the configuration-state functions are optimized by minimizing the variance of the local energy.[16] The resulting wave functions had rms fluctuations of local energy that range from 0.021 H* for $N=2$ to 0.255 H* for $N=13$.

III. RESULTS

Using these optimized wave functions for importance sampling, we perform fixed-node diffusion Monte Carlo calculations. We attempt to establish the accuracy of the fixed-node energies obtained with our trial wave functions by comparing them to energies from exact diagonalization studies and also by performing internal checks within our calculations. Unfortunately, although there exist several papers on exact diagonalization,[7,8] the results are usually presented in plots, rather than in tables. The only number we know of is in Ref. 17, who give an energy of 26.82 meV for $N=3$, which they credit to Hawrylak and Pfannkuche.[8] Starting from a single Slater determinant of LDA orbitals (constructed from the spin-up and spin-down $|n,l\rangle=|0,0\rangle$ states and the spin-up $|n,l>=|0,1\rangle$ state), we obtain a fixed-node DMC energy of 26.8214(36) meV, using their model parameters ($m^*=0.067m_e$, $\epsilon=12.4$, and $\hbar\omega=3.37$ meV), which is indistinguishable from the exact energy to the number of digits quoted. We attempted also to estimate the fixed-node error by varying the orbitals in the determinants and by varying the number of determinants. For $N=7$, QMC calculations using LDA and LSDA orbitals were performed. The LSDA orbitals yielded better VMC results (the energy was lowered by 57 mH* and the fluctuations of the local energy by 7 mH*) but the DMC energies were unchanged within statistical uncertainty. We checked the dependence of the energy on the number of configuration-state functions for the first excited state of the $N=9$ dot. Somewhat to our surprise, energies of the one-configuration (three-determinant) and the two-configuration (five-determinant) wave functions agreed to within 1 mH*, not only within the DMC method but also within the VMC method.

TABLE II. Comparison of ground-state energies (in H*) for the dots with $2 \leq N \leq 13$ computed by the Hartree-Fock, LSDA, VMC, and DMC method. Also shown are the LSDA errors in the energy, $\Delta E_{\rm LSDA}=E_{\rm LSDA}-E_{\rm DMC}$, which are much smaller than the HF errors $E_{\rm HF}-E_{\rm DMC}$. The numbers in parentheses are the statistical uncertainties in the last digit.

N	$E_{\rm HF}$	$E_{\rm LSDA}$	$E_{\rm VMC}$	$E_{\rm DMC}$	$\Delta E_{\rm LSDA}$
2	1.1420	1.04685	1.02205(7)	1.02162(7)	0.02523(7)
3	2.4048	2.2631	2.5022(3)	2.2339(3)	0.0292(3)
4	3.9033	3.6864	3.7252(4)	3.7135(5)	0.0276(7)
5	5.8700	5.5735	5.5473(5)	5.5336(3)	0.0263(7)
6	8.0359	7.6349	7.6214(3)	7.5996(8)	0.0353(8)
7	10.5085	10.0718	10.0587(9)	10.0361(8)	0.0357(8)
8	13.1887	12.7276	12.7119(7)	12.6903(7)	0.0373(7)
9	16.1544	15.6190	15.6039(9)	15.5784(7)	0.0406(7)
10	19.4243	18.7636	18.7568(9)	18.7244(5)	0.0392(5)
11	22.8733	22.1114	22.1128(9)	22.0750(4)	0.0364(4)
12	26.5490	25.6756	25.6792(11)	25.6548(7)	0.0208(7)
13	30.4648	29.5363	29.5430(14)	29.4942(7)	0.0421(7)

A. Ground-state energies

The ground-state energies are listed in Table II and compared with results of HF and LSDA calculations using the Tanatar-Ceperley parametrization for the correlation energy.[25] The HF energies are 0.12–0.97 H* higher than the DMC energies whereas the LSDA energies are only 0.021–0.042 mH* (0.25–0.50 meV) higher. In contrast, in atoms and molecules the Hartree-Fock total energy is considerably better than the LSDA total energy. There are two likely reasons for this difference. First, the Hartree-Fock treats exchange energy exactly while completely ignoring correlation, whereas in the LSDA both exchange and correlation are approximated. In atoms and molecules, the exchange energy E_x is much larger than the correlation energy E_c, but for the dots it is not, e.g., $E_x/E_c \approx 30$ for a neon atom but E_x/E_c

≈ 4 for an $N=10$ dot. The second reason is that the dots are more homogeneous than atoms or molecules and so the local-density approximations to E_x and E_c work better. Note also that the HF errors increase monotonically with electron number but the LSDA errors do not show any obvious trend.

B. Excited-state energies

In Table I we list the low-lying excitation energies for the $N=4,\ldots,11$ dots. Koskinen *et al.*[13] find that the lowest excitation energies from LSDA calculations are 11.5 mH* and 2.31 mH* for $N=8$ and 10 dots, respectively, whereas our DMC calculations show that the corresponding lowest excitation energies are 22 mH* and 2 mH*. They claim that these lowest excited states have a spin density wave even though $S=0$, but in fact this is just an artifact due to these LSDA wave functions not being eigenstates of $\hat{S}^2$, as pointed out by Hirose and Wingreen.[14] For both the $N=8$ and the $N=10$ dots, the first excited-state LSDA wave functions are in fact linear combinations of $(L,S)=(2,1)$ and the $(L,S)=(2,0)$ wave functions. In general, the single-determinant LSDA wave functions are eigenstates of $\hat{S}_z$, but they are eigenstates of $\hat{S}^2$ only when $|\hat{S}_z|$ has the maximum value consistent with filling the lowest $N/2$ orbitals and the exclusion principle. In other cases it is necessary to have more than one determinant in order to have the correct spin symmetry. Single-particle levels in a parabolic potential with the same value of $2n+|l|+1$ are degenerate. However, the self-consistent LSDA potential is not parabolic, and consequently of two levels with the same $2n+|l|+1$, the LSDA orbital with the larger value of $|l|$ is lower than the other. This serves to explain the ordering of levels for the dots where N differs from a closed shell by 1. For example, the $(L,S)=(2,1/2)$ state lies lower than the $(L,S)=(0,1/2)$ state in the $N=7$ dot but the order is reversed in the $n=11$ dot because the $(n,l)=(0,\pm 2)$, LSDA single-particle level lies below the $(n,l)=(1,1)$ level.

C. Change in electrochemical potential

The DMC estimates for the change in electrochemical potential Δ_N (in meV) as a function of N are reported in Fig. 1 together with those from LSDA and HF calculations. We see structures and peaks at electron numbers 2, 4, 6, 9, and 12 in agreement with the experiments of Ref. 5. In the independent-particle model with a parabolic potential, Δ_N has peaks of magnitude ω at $N=2,6,12,\ldots$, corresponding to closed shells, and is 0 elsewhere. Additional features are due to the electron-electron interaction. It is difficult to make a more detailed comparison between experiments and theory because of uncertainties in the Hamiltonian. In particular, the external potential may not be strictly parabolic and our assumption that ω is independent of N may not be an accurate description of the experimental situation.

D. Correlation energies

In Fig. 2 we plot the DMC correlation energy calculated as the difference between the DMC energy and the HF energy[26] as a function of the electron number N. The dashed line indicates the LSDA correlation energy. From the figure one sees that the LSDA overestimates the correlation energy by 10%–15% almost independently of N. The LSDA overestimate of the correlation energy is smaller than in atoms and jellium spheres, where it is as much as 100% (Ref. 27) and 30% (Ref. 23), respectively.

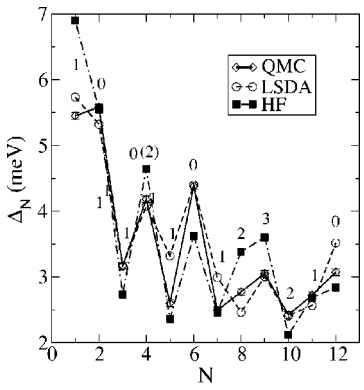

FIG. 1. Change in electrochemical potential Δ_N as a function of the number of electrons, N, in the dot. The numbers in the plot are the DMC spin polarizations $2S_z=N\uparrow-N\downarrow$. The LSDA and HF spin polarization for the $N=4$ dot is given in parentheses; for all other N they are the same as for the DMC method.

E. Hund's first rule

From Table I we see that Hund's first rule, according to which the total spin of the ground state takes the maximum value consistent with electrons being in the same shell and the exclusion principle, is satisfied for all values of N studied in this work, except for $N=4$. For $N=4$ the $|L,S\rangle=|0,0\rangle$ state is just 2.2 mH* or 0.026 meV lower than the $|0,1\rangle$ state, so a small change in the Hamiltonian, e.g., an increase in the spring constant of the confining potential ω, could alter the ordering of these two states. Our result for the $N=4$ dot is in qualitative agreement with the QMC results of Bolton[19] but they find that the the singlet state is lower than the triplet by a larger amount (1.5 meV) than we do, for Hamiltonian parameters that are close to, but not equal to, the the ones we use. However, our result disagrees with our LSDA calculations which find no violations of Hund's rule for $N\leqslant 13$ as well as the earlier LSDA calculations[13] which found that, for dots with even N, Hund's rule is satisfied for $N\leqslant 22$, but violated for $N=24$. On the other hand, spin-and-space unre-

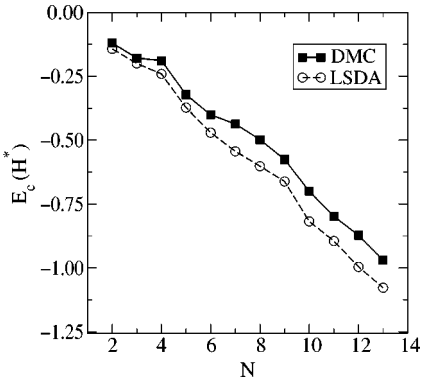

FIG. 2. Correlation energies E_c for circular dots computed with the DMC (solid squares) and LSDA (open circles) methods.

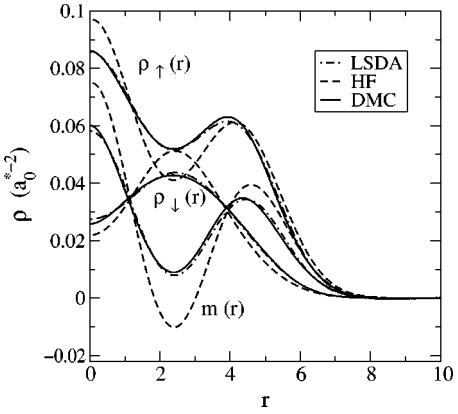

FIG. 3. Spin densities $\rho_\uparrow(r),\rho_\downarrow(r)$ and magnetization $m(r)=\rho_\uparrow(r)-\rho_\downarrow(r)$ as a function of distance from the center for the ground state of the $N=9$ dot. Solid lines, DMC; dotted-dashed lines, LSDA, dashed line, HF. The LSDA spin densities for this state agree well with the DMC spin densities but the HF spin densities have considerably larger oscillations.

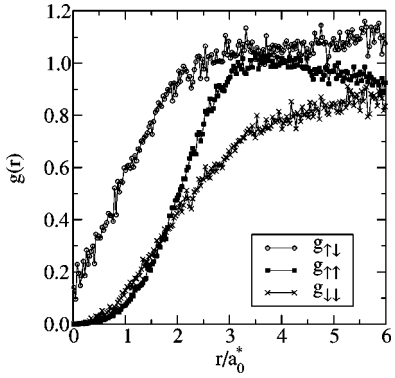

FIG. 4. Electron pair correlation functions, from the variational MC method, of the ground state of the $N=9$ dot. The first electron is at the center of the dot. Open circles, $g(r)_{\uparrow\downarrow}$; solid squares, $g(r)_{\uparrow\uparrow}$; crosses, $g(r)_{\downarrow\downarrow}$.

stricted Hartree Fock (sS-UHF) calculations[12] predict that Hund's rule is violated not only for $N=4$ but also for $N=8$ and $N=9$. It should be noted that the sS-UHF calculations were performed for a smaller value, $\lambda=1.48$, of the dimensionless ratio of the Coulomb interaction strength to the confining potential, defined in Sec. II A, than our calculations which were for $\lambda=1.89$. Since, according to Ref. 12, Hund's rule violations are less likely for smaller values of λ, it is clear that the difference is not due to the different value of λ. Experimental evidence indicates that Hund's rule is satisfied for $N=4$ circular dots[5,6] but that a small elliptical deformation is sufficient for the singlet and triplet energies to cross,[6] thereby confirming our finding that the two states are very close in energy. Given the uncertainty in the experimental Hamiltonian and the near degeneracy of the two states, it is not surprising that we find that the the singlet state is lowest whereas the experimental finding is that the triplet is lowest for the circular dot. The results of two exact diagonalization studies are also relevant in this context: Eto[7] found that a small magnetic field is sufficient to switch the order of the states whereas Hirose and Wingreen[14] find that a small quartic term in the Hamiltonian has the same effect.

F. Spin densities

In Fig. 3 we compare the spin densities $\rho_\uparrow$ and $\rho_\downarrow$ and the magnetization $m(r)=\rho_\uparrow(r)-\rho_\downarrow(r)$ for the $N=9$ ground state obtained from the DMC and LSDA methods. In this case the LSDA wave function is an eigenstate of $\hat{S}^2$. The agreement of the curves is impressive and extends to the whole region of r, including the edge, where the density gradients are large. The same kind of agreement with the LSDA was also obtained in the case of variational Monte Carlo densitites[23] of jellium spheres. In general, it appears that the LSDA gives accurate spin densities in those cases that the Kohn-Sham wave function has the correct spin symmetry. In contrast the HF spin densities show much larger oscillations than the DMC spin densities. The same behavior has previously been noticed for atoms, but to a much lesser degree.[28]

Yannouleas and Landman plot in Fig. 2 of Ref. 12 the charge density of a closed-shell $N=6$ dot obtained from a sS-UHF calculation. They find that the charge density of a dot with a dimensionless interaction strength of $\lambda=1.48$ has a noncircular charge density that they refer to as a Wigner crystallized state, although the usual definition of Wigner crystallization refers to the occurrence of long-range order in the two-body density rather than short-range order in the one-body density. Since the ground state of the $N=6$ dot is of ^1S symmetry, it is apparent that the density must be circularly symmetric and their result is an artifact of their computational method. In this context it should be noted that for very large values of λ one cannot immediately rule out the possibility that the single-particle picture breaks down completely and that the ground state is not of ^1S symmetry. Also, in the presence of a strong magnetic field the single-particle levels will reorder and the ground state need not have ^1S symmetry. Finally, it should be noted that other authors[29] have considered models for dots in which the confining potential itself can deform and therefore not be circularly symmetric. In this case, of course, the ground state density of the $N=6$ dot need not be circularly symmetric either.

G. Pair-correlation functions

In Fig. 4 we show the spherical average of the electron-electron pair-correlation functions $g_{\sigma_1,\sigma_2}(\mathbf{r}_1,\mathbf{r}_2)$ in the $N=9$ case. The different behavior for pairs with parallel and antiparallel spin is due to the fact that the wave function vanishes when parallel-spin electrons coalesce but not when antiparallel-spin electrons coalesce. For $N=9$, it follows from Hund's rule that there are twice as many up-spin electrons as down-spin electrons. This is reflected in the shape of the $g_{\uparrow\uparrow}$ and $g_{\downarrow\downarrow}$ curves.

IV. CONCLUSIONS

In conclusion, we have calculated QMC ground-state energies, excitation energies, correlation energies, change in electrochemical potential due to adding an electron, spin densities, and pair-correlation functions for circular quantum dots with $N\leqslant 13$ electrons and compared them to the corresponding quantities obtained from HF and LSDA calcula-

tions. We find that HF energies are in error by 0.12–0.97 H* but LSDA energies by only 0.021–0.042 H*. However, even the LSDA energies are not sufficiently accurate to give reliable excitation energies or changes in the electrochemical potential. The LSDA correlation energies differ from the DMC ones by $\simeq$ 10%–15%. Hund's first rule is found to be satisfied for all dots up to $N \leqslant 13$, for the Hamiltonian parameter values employed, except for $N=4$ which has a near degeneracy. The LSDA spin densities are in remarkably good agreement with DMC spin densities for those cases where the Kohn-Sham wave function is an eigenstate of $\hat{S}^2$ but the HF densities have oscillations that are too large. Finally, the pair-correlation functions may be of utility in constructing more accurate energy density functionals than the LSDA for two-dimensional systems.

ACKNOWLEDGMENTS

We thank Ll. Serra for providing us with the HF code and M. Barranco for useful conversations. This work was partially supported by INFM, MURST, and Sandia National Laboratory. The calculations were carried out on the IBM-SP2 at Cornell Theory Center and on the Cray-T3E at CINECA with an ICP-INFM grant.

[1] M. A. Kastner, Rev. Mod. Phys. **64**, 849 (1992); Phys. Today **46**(1), 24 (1993).
[2] R. C. Ashoori, Nature (London) **379**, 413 (1996); L. P. Kouwenhoven, T. H. Oosterkamp, M. W. Danoesastro, M. Eto, D. G. Austing, T. Honda, and S. Tarucha, Science **278**, 1788 (1997).
[3] U. Meirav, M. A. Kastner, and S. J. Wind, Phys. Rev. Lett. **65**, 771 (1990).
[4] R. C. Ashoori, H. L. Stormer, J. S. Weiner, L. N. Pfeiffer, S. J. Pearton, K. W. Baldwin, and K. W. West, Phys. Rev. Lett. **68**, 3088 (1992).
[5] S. Tarucha, D. G. Austing, T. Honda, R. J. van der Hage, and L. P. Kouwenhoven, Phys. Rev. Lett. **77**, 3613 (1996); Jpn. J. Appl. Phys., Part 1 **36**, 3917 (1997); S. Sasaki, D. G. Austing, and S. Tarucha, Physica B **256**, 157 (1998).
[6] D. G. Austing *et al.*, Phys. Rev. B **60**, 11 514 (1999).
[7] M. Eto, Jpn. J. Appl. Phys., Part 1 **36**, 3924 (1997).
[8] P. A. Maksym and T. Chakraborty, Phys. Rev. Lett. **65**, 108 (1990); D. Pfannkuche, V. Gudmundsson, and P. A. Maksym, Phys. Rev. B **47**, 2244 (1993); P. Hawrylak and D. Pfannkuche, Phys. Rev. Lett. **70**, 485 (1993); J. J. Palacios, L. Moreno, G. Chiappe, E. Louis, and C. Tejedor, Phys. Rev. B **50**, 5760 (1994); T. Ezaki, N. Mori, and C. Hamaguchi, *ibid.* **58**, 6428 (1997).
[9] A. Kumar, S. E. Laux, and F. Stern, Phys. Rev. B **42**, 5166 (1990).
[10] M. Fujito, A. Natori, and H. Yasunaga, Phys. Rev. B **53**, 9952 (1996).
[11] H. M. Muller and S. Koonin, Phys. Rev. B **54**, 14 532 (1996).
[12] Constantine Yannouleas and Uzi Landman, Phys. Rev. Lett. **82**, 5325 (1999). In this paper the sS-UHF calculation predicts that Hund's rule is satisfied for $N=4$ but it was conveyed to us in personal communication that this is a typographical error.
[13] M. Koskinen, M. Manninen, and S. M. Reimann, Phys. Rev. Lett. **79**, 1389 (1997).
[14] K. Hirose and N. S. Wingreen, Phys. Rev. B **59**, 4604 (1999).
[15] M. Ferconi and G. Vignale, Phys. Rev. B **50**, 14 722 (1994); E. Lipparini, N. Barberan, M. Barranco, M. Pi, and Ll. Serra, *ibid.* **56**, 12 375 (1997); M. Pi, M. Barranco, A. Emperador, E. Lipparini, and Ll. Serra, *ibid.* **57**, 14 783 (1998); O. Steffens, U. Rossler, and M. Suhrke, Europhys. Lett. **42**, 529 (1998); O. Steffens, M. Suhrke, and U. Rossler, *ibid.* **44**, 222 (1998).
[16] C. J. Umrigar, K. G. Wilson, and J. W. Wilkins, in *Computer Simulation Studies in Condensed Matter Physics: Recent Developments*, edited by D. P. Landau and H. B. Schüttler (Springer-Verlag, Berlin, 1988); Phys. Rev. Lett. **60**, 1719 (1988).
[17] A. Harju, V. A. Sverdlov, R. M. Nieminen, and V. Halonen, Phys. Rev. B **59**, 5622 (1999).
[18] J. Shumway, L. R. C. Fonseca, J. P. Leburton, R. M. Martin, and D. M. Ceperley, http://xxx.lanl.gov/abs,cond-mat/cond-mat/9912166 (unpublished).
[19] F. Bolton, Phys. Rev. B **54**, 4780 (1996).
[20] C. H. Mak, R. Egger, and H. Weber-Gottschick, Phys. Rev. Lett. **81**, 4533 (1998); R. Egger, W. Husler, C. H. Mak, and H. Grabert, *ibid.* **82**, 3320 (1999).
[21] C. J. Umrigar, M.P. Nightingale, and K. J. Runge, J. Chem. Phys. **99**, 2865 (1993).
[22] V. Fock, Z. Phys. **47**, 446 (1928); C. G. Darwin, Proc. Cambridge Philos. Soc. **27**, 86 (1930).
[23] P. Ballone, C. J. Umrigar, and P. Delaly, Phys. Rev. B **45**, 6293 (1992).
[24] C. J. Huang, C. Filippi, and C. J. Umrigar, J. Chem. Phys. **108**, 8838 (1998).
[25] B. Tanatar and D. M. Ceperley, Phys. Rev. B **39**, 5005 (1989).
[26] We are neglecting here the small difference between the density functional and the quantum chemistry definitions of the correlation energy.
[27] J. P. Perdew and A. Zunger, Phys. Rev. B **23**, 5048 (1981).
[28] Claudia Filippi, Xavier Gonze, and C. J. Umrigar, in *Recent Developments and Applications of Density Functional Theory*, edited by J. M. Seminario (Elsevier, Amsterdam, 1996).
[29] S. M. Reimann, M. Koskinen, J. Helgesson, P. E. Lindelof, and M. Manninen, Phys. Rev. B **58**, 8111 (1999).